AIP | Journal of Applied Physics

An ab-initio study of electronic and optical properties of corundum Al2O3 doped with Sc, Y, Zr, and Nb

A. F. Lima, J. M. Dantas, and M. V. Lalic

Citation: J. Appl. Phys. **112**, 093709 (2012); doi: 10.1063/1.4764317
View online: http://dx.doi.org/10.1063/1.4764317
View Table of Contents: http://jap.aip.org/resource/1/JAPIAU/v112/i9
Published by the AIP Publishing LLC.

An *ab-initio* study of electronic and optical properties of corundum Al_2O_3 doped with Sc, Y, Zr, and Nb

A. F. Lima, J. M. Dantas, and M. V. Lalic[a)]
Universidade Federal de Sergipe, Departamento de Física, P.O. Box 353, 49100-000, São Cristovão – SE, Brazil

(Received 15 August 2012; accepted 9 October 2012; published online 5 November 2012)

Ab-initio calculations based on density functional theory have been employed to study the structural, electronic, and optical properties of yttrium (Y), scandium (Sc), zirconium (Zr), and niobium (Nb) doped α-Al_2O_3 with corundum structure. Exchange and correlation effects between electrons have been treated by generalized gradient approximation within the Perdew-Burk-Ezrenhof parameterization and by recently developed Tran-Blaha modified Becke-Johnson approach. Most attention in the work has been paid to the impurity d states, whose energy splitting has been analyzed in terms of the crystal field theory and whose influence on the gap size and the offset of the bands around it has been carefully evaluated. The influence of these states on modification of the optical absorption edge and the static dielectric constant of the doped systems has been also studied. It is concluded that only the Y doped α-Al_2O_3 (1) preserves the size of the band gap of the pure alumina, (2) does not change significantly the band offset around it, and (3) elevates the value of the static dielectric constant of the compound. These three conditions, necessary for usability of the doped material as a high-ε dielectric gate, are not satisfied by the Sc-, Zr-, and Nb-doped alumina compounds. Therefore, only the Y-doped α-Al_2O_3 exhibits potential to be further explored for employment in the semiconductor industry. © *2012 American Institute of Physics*. [http://dx.doi.org/10.1063/1.4764317]

I. INTRODUCTION

The alumina (Al_2O_3) attracts significant scientific attention for decades because of the large number of application in science and technology. It can crystallize in different crystal structures depending on the growth conditions. The most stable is the structure of corundum, known as the α-Al_2O_3. During the last few decades, the α-Al_2O_3 has been widely studied both theoretically and experimentally, either in its pure or defective (doped) form.[1–4]

Alumina is a very good isolator. This property makes it interesting for semiconductor industry which constantly searches for new materials to build dielectric gates in transistors and integrated circuits.[5–10] The objective of this search is to further diminish the size of transistors by improving the capacitance (c) of their capacitors. As $c \sim \varepsilon/d$, and d (the distance between the capacitor's plates) cannot be made arbitrarily small due to the leakage of current via electron tunnelling, the only solution is to employ some material with very high dielectric constant ε between the plates.

Various studies indicate the alumina as one of the most proper candidates for such an employment:[5–7] it has a wide band gap (8.8 eV), similar band offset as the SiO_2 (dielectric material most widely used in electronics) and high dielectric constant ($\varepsilon = 9$), which can be elevated even more by appropriate doping of the pure material. The appropriate doping should meet two basic criteria: (1) it must not change too much the band gap of the pure material nor the band offset around it, and (2) it must cause the increment of the dielectric constant, mostly for low energies. In 2002, the theoretical study of Haverty *et al.*[8] showed that the presence of certain transition metals (Y, Sc) within the alumina with orthorhombic structure (κ-Al_2O_3) maintains the gap value and increases the dielectric constant, while the presence of others (Zr, Nb) diminishes the gap and "spoils" the dielectric properties of the host. One year after, in 2003, Jung *et al.*[9] confirmed this theoretical prediction by studying experimentally the amorphous alumina doped with Y, Sc, Zr, and Nb.

The two mentioned studies impose the question if the same impurities produce the same effects when inserted into the most stable α-alumina. With a principal motivation to clarify this point, we performed the thorough theoretical study of structural, electronic, and optical properties of α-Al_2O_3 which contains isolated transition metal impurities of Y, Sc, Zr, and Nb that substitute the Al atom in the host crystalline matrix.

There exist other theoretical studies of α-Al_2O_3 doped with the mentioned transition metal impurities, but with incomplete or even controversial conclusions about electronic structure and band gaps of the doped systems. For example, Samantaray *et al.*[10] calculated the electronic structure of α-Al_2O_3 doped with Y, Sc, Zr, Hf, and Ta. They predicted that the Y presence practically does not change the gap size of the pure system, while the other impurities reduce the gap by 0.33 eV (Sc), 0.52 eV (Zr), 0.60 eV (Hf), and 0.76 eV (Ta). They, however, considered high concentration of impurities ($Al_{1.8}T_{0.2}O_3$) and did not report any details about relaxation of the structure around them. Aliabad *et al.*[11] studied the electronic structure of α-Al_2O_3 doped with Zr, Ti, and Hf and concluded that the Zr and Hf presence increase the gap size, while the Ti decreases it. They simulated even higher concentration of impurities

a)Electronic mail: mlalic@ufs.br.

($Al_{1.5}T_{0.5}O_3$), and seem not performed relaxation of the structure near the defect. Ching *et al.*[12] investigated seriously the electronic structure of Y containing α-Al_2O_3 (where 2% of Al was substituted by Y) and concluded that the band gap is lower by only 0.15 eV. They, however, performed structure relaxation only for the first and second neighbourhood around the impurity.

The present work collects into one place the relevant pieces of information about the structural, electronic, and optical properties of the Al_2O_3:M (M = Sc, Y, Zr, Nb) compounds and answers the question about the dielectric usability of the defective systems. Our conclusion is that only the Y presence in the α-Al_2O_3 preserves the size of the band gap of the pure alumina, does not change much the band offset around it, and elevates the value of the static dielectric constant. Thus, only the Y-doped α-Al_2O_3 has potential to be further explored for eventual employment in the semiconductor industry.

II. CALCULATIONS DETAILS

Here, we consider the α-Al_2O_3 which crystallizes in corundum structure, with the hexagonal Bravais lattice and the space group R-3C (167). The primitive unit cell contains two molecules of Al_2O_3, i.e., 10 atoms, while the local coordination of Al consists of 6 oxygen atoms arranged in the vertices of distorted octahedron.[13]

In this work, we study the five different systems. All of them have been modeled on the basis of one super-cell consisting of eight primitive α-Al_2O_3 unit cells (with 80 atoms inside). The pure alumina crystal is constructed by infinite repetition of this supercell. In the case of defective systems, the super-cell was modified by replacing one Al atom in its center by an impurity M atom. The four doped systems Al_2O_3:M (M = Sc, Y, Zr, Nb) were then constructed by infinite repetition of this modified super-cell, simulating compounds with chemical formula $Al_{2-x}M_xO_3$, where x = 0.0625. This way the defective systems contain small concentration of impurities (1.25% of total number of atoms, or 6% of all Al atoms), meeting approximately our objective to treat the presence of isolated impurities in alumina.

As a computational tool, we employed the full potential linear augmented plane wave (FP-LAPW) method[14] based on density-functional theory (DFT)[15] and implemented in WIEN2k computer code.[16] In this method, the electronic wave function, charge density, and crystal potential are expanded in terms of spherical harmonics inside the non-overlapping spheres centered at each nuclear position (atomic spheres), and in terms of plane waves in the rest of the space (interstitial region). The radii of atomic spheres (in atomic units) were chosen to be 1.8 for the Al, Y, Sc, Zr, and Nb, and 1.5 for O. Inside atomic spheres, the partial waves were expanded up to $l_{max} = 6$, while the number of plane waves in the interstitial was limited by the cut-off at $K_{max} = 7.0/R_{MT}$. The augmented plane waves were utilized as a basis set. The charge density was Fourier expanded up to $G_{max} = 14$. The $^{13}Al—2p^6 3s^2 3p^1$, $^{8}O—2s^2 2p^4$, $^{39}Y—4s^2 4p^6 4d^1 5s^2$, $^{21}Sc—3p^6 3d^1 4s^2$, $^{40}Zr—4s^2 4p^6 4d^2 5s^2$, and the $^{41}Nb—4s^2 4p^6 4d^4 5s^1$ electronic states were considered as valence ones, and treated within the scalar-relativistic approach, whereas the core states were relaxed in a fully relativistic manner. Exchange and correlation effects were treated in two different ways. For optimization of crystal structures, relaxation of atomic positions, and calculation of defect formation energies, we used the generalized-gradient approximation (GGA) within the Perdew-Burk-Ezrenhof (PBE) parameterization[17] (in further text we refer to this approach as the "PBE calculations," or the "PBE approach"). These calculations were performed with the 6 k-points in the irreducible part of the Brillouin zone (IBZ). The electronic structure and optical properties were calculated with both the PBE and the modified Becke-Johnson (mBJ) potential[18] (in further text: "mBJ calculations" or the "mBJ approach"). The latter has been proven to provide better description of band gap and optical properties for various classes of insulating materials.[19–21] In the case of the mBJ calculations, the IBZ was sampled with 12 k-points because we perceived that this approach is more sensitive on the number of k-points. In both cases, the good convergence of the results has been achieved (less then 10^{-4} Ry and 10^{-5} *e* for energy and charge convergence, respectively).

III. RESULTS AND DISCUSSION

A. Structure relaxation and defect formation energies

We started our calculations with computational optimization of all considered crystalline systems. The lattice parameters of the pure alumina were calculated to be $a = b = 4.8211$ Å and $c = 13.1609$ Å, being 4% larger than experimental ones.[13] The supercell lattice parameters were defined by doubling these values, both for the pure and the defective systems ($a = b = 9.6422$ Å and $c = 26.3218$ Å). All atomic positions in the unit cells (not just those around the impurities) were allowed to relax until the equilibrium positions were reached (in which the forces sensed by each of the atoms were lesser than 3 mRy/a.u.). The lattice parameters for the defective systems were kept unchanged since we considered that the small percentage of impurities should not affect them too much.

Table I shows the calculated relaxed distances between the atoms situated at the Al site, which we shall call the M

TABLE I. Calculated interatomic distances between the atom at the M site (M = Al, Sc, Y, Zr, Nb) and its first and second nearest neighbor O atoms, as well as between the M atom and its third nearest neighbor Al atoms. The experimental data are provided for the pure alumina only.

	Neighbor's					
	1st		2nd		3rd	
	This work	Expt.[a]	This work	Expt.[a]	This work	Expt.[a]
Al	1.878	1.855	1.997	1.972	2.687	2.655
Sc	1.992		2.135		2.782	
Y	2.075		2.277		2.923	
Zr	2.066		2.195		2.849	
Nb	2.053		2.132		2.778	

[a]Reference 13.

site, and the atoms in their nearest surroundings. M = Al in the case of the pure, and M = Sc, Y, Zr, or Nd in the case of the defective systems. The first coordination sphere of the M site consists of the six O atoms situated at the vertices of distorted octahedron around it: three of them are closer to, and other three are farther from the M atom. The former are denoted the first neighbors and the latter the second neighbors of the M. The second coordination sphere of the M site consists of the 4 Al atoms irregularly distributed around it. The Al atom that is nearest to the M site is designated as the third neighbor.

Table I demonstrates that the calculated interatomic distances agree well with experimental data in the case of the pure alumina. To the best of our knowledge, such experimental data are not available for the defective systems. For them, our calculations predict an increment of the size of the first and the second coordination sphere around the impurity, in accordance with the size of the ionic radius of the impurity. In Ref. 12, the authors employed the first-principles approach to calculate interatomic distances for the Al_2O_3:Y system. They got the values: 2.006, 2.094, and 2.679 Å for the Y-O (first neighbors), Y-O (second neighbors), and Y-Al (third neighbors) distances, respectively. These values do not agree very well with ours, but in our calculations all atoms in the unit cell were relaxed while in the Ref. 12 the relaxation has been limited to the neighbors up to the second coordination sphere around the Y.

The defect formation energies, E_d, required for substitution of one Al atom for an impurity atom, were calculated as the difference in the total energies of (i) a perfect super-cell plus a free impurity atom at infinity and (ii) an impurity-contained super-cell plus a free aluminum atom at infinity. The energies of the perfect and the imperfect super-cells were calculated using the same computation parameters (number of k-points, atomic sphere radii, etc.). For the computation of energies of the free atoms, we considered an infinite structure consisting of very large empty cubic unit cells (with lattice parameter of 30 atomic units) with the atoms in their centers. The free atom energies were then calculated as the unit cell energies, using the spin-polarized approach and with one k-point in the IBZ. The results are presented in Table II.

It should be noted that the negative sign of E_d means that the energy of the perfect system + free impurity is more negative than the energy of the defective system + free Al. In this case, to substitute the Al atom an additional energy is required. Having this in mind, we conclude that the Y and Sc can be more easily incorporated into α-Al_2O_3 than the Zr and Nb. This is justified by the fact that both Sc and Y have the same oxidation state (+3) as the Al atom, while the Zr (+4) and Nb (usually +5) have not. The only surprise is that the Y insertion is energetically more profitable than the Sc insertion, considering the fact that the latter has the ionic radius more similar to the ionic radius of the Al. The explanation lies in specific electronic structures of the Al_2O_3:Y and the Al_2O_3:Sc compounds: as will be shown in Sec. III B, the Sc presence changes the overall band structure of the host α-Al_2O_3 much more than the Y presence, and this costs energy.

TABLE II. Calculated defect formation energies (E_d) of α-Al_2O_3 doped with Y, Sc, Zr or Nb, which substitute the Al atom.

	Defect formation energy (eV)	
	Thiswork	Ching *et al.*[12]
Al_2O_3: Y	1.56	4.79
Al2O3: Sc	0.18	
Al2O3: Zr	−0.14	
Al2O3: Nb	−0.82	

B. Electronic structure

As mentioned in Sec. II, the electronic structure of the Al_2O_3:M (M = Sc, Y, Zr, Nb) compounds has been calculated using two different exchange-correlation potentials: the PBE and the mBJ. The resulting total and projected density of electronic states (TDOS and PDOS, respectively) of the PBE calculations are presented in Figure 1, while the results of the mBJ calculations are shown in Figures 2 and 3. Since the Sc and Y impurities do not exhibit magnetic moments, their DOS is not represented as a spin polarized. The Zr and Nb impurities, on the other hand, exhibit non-zero magnetic moments. For this reason, the DOS of the Al_2O_3:Zr and the Al_2O_3:Nb is represented for both spin components.

The comparison of the TDOS in Figures 1–3 leads to the obvious conclusion that the PBE and the mBJ calculations produce quantitatively different results (see Table III). The size of the pure alumina gap is different, the Zr and Nb magnetic moments are slightly different, and the splitting between the impurity-induced peaks is much more pronounced in the mBJ TDOS. But, on the other hand, the form and the composition of the alumina valence band (mostly O 2p-states) and conduction band (mixture of the O 2p- and the Al s-states) are practically the same. Further, all impurity-induced peaks that are present in the PBE TDOS are also present in the mBJ TDOS, with the same orbital decomposition and the relative positions within the gap (although their widths and absolute positions are different). Considering these facts, we conclude that both PBE and mBJ calculations produce qualitatively similar results, which can be interpreted in the same way.

The energy splitting of the impurity *d*-states can be understood in terms of the crystal field theory. The impurity situated at the Al site senses the influence of trigonally distorted octahedral crystal field of six neighbouring O ions. The octahedral (cubic) crystal field splits the 10-fold degenerate *d* energy level into the lower energy T_{2g} (6-fold degenerate) and the higher energy E_g (4-fold degenerate) level. The trigonal distortion lowers the symmetry and additionally splits the T_{2g} level into the 4-fold degenerate E level (lower energy) and doubly degenerate A level (higher energy). This splitting is nicely exhibited in Figure 2 in the case of the Sc *d*-states (peaks numbered 1 and 2) and the Y *d*-states (peaks numbered as 3 and 4). The peaks 1 and 3 correspond to the T_{2g}, while the peaks 2 and 4 to the E_g energy levels. The two lowest graphs of Figure 2 show that the T_{2g} level also splits: the $d_{xz} + d_{yz}$ states (2 electrons) and the $d_{x2y2} + d_{xy}$ states (2 electrons) form the E energy level, while the d_z^2 states (2

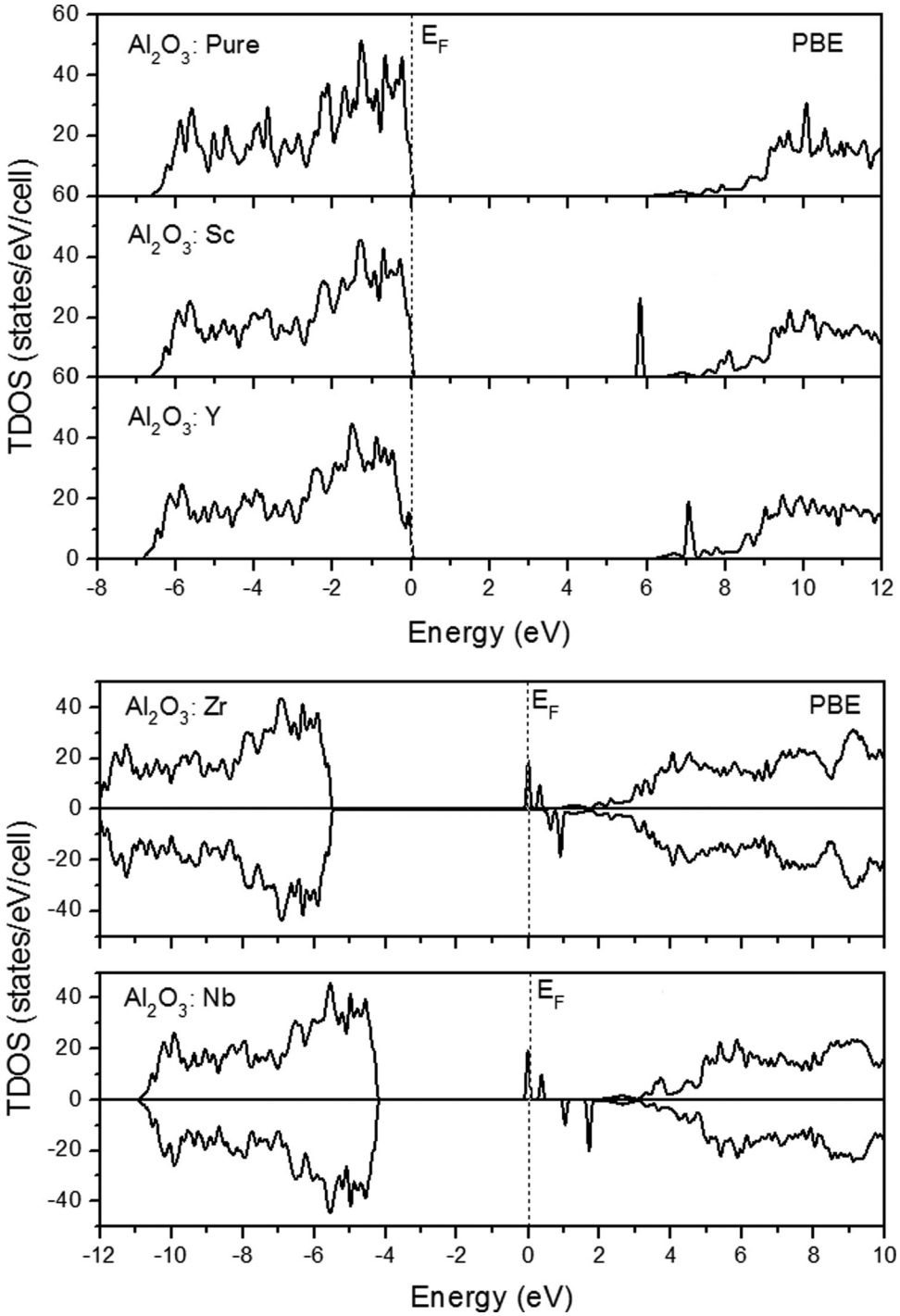

FIG. 1. The TDOS of the pure and the four defective alumina systems, calculated using the PBE exchange-correlation potential. The peaks inside the gap, as well as the ones appended to the conduction band bottom of the host alumina spectrum, originate from the d-states of the impurity atoms.

electrons) form the A energy level. It should be noted that specific orbital characters of the states that realize the E, A, and E_g levels depend on orientation of the local coordinate system whose origin is at the centre of the impurity atom. All the Sc and the Y *d*-states are empty: their unique *d*-electron is delocalized when incorporated into the host matrix. It is donated, together with the two s-electrons, to the three nearest neighbour oxygens. The cubic field splitting between the T_{2g} and the E_g levels is significant: about 1.7 and 2.1 eV for the Sc and Y, respectively, while the trigonal splitting of the T_{2g} level (between the E and A) is very small: about 0.1 and 0.2 eV for the Sc and the Y, respectively.

The Zr and Nb accommodate more than one electron in their *d*-shells, and the splitting between their *d* energy levels is more pronounced. Entering at the trivalent Al site, both Zr and Nb release two *s*- and one *d*-electron in order to satisfy bonds to the nearest oxygens. Thus, the Zr keeps one, and the Nb keeps two electrons localized in the *d*-shell. These electrons are loosely bounded and their energy is high in relation with the top of the valence band. Figure 3 shows the arrangement of the *d* energy levels of the Zr and Nb impurities inside the alumina band gap. The Zr *d*-electron is situated within the band number 1, which is half-populated, while the two Nb *d* electrons are accommodated within the band number 6, which is completely full. For the majority spin (spin-up), the trigonal splitting between the E and A energy levels is very large (splitting between the peaks 1 and 2, and the 6 and 7 in Fig. 3), while for the minority spin the

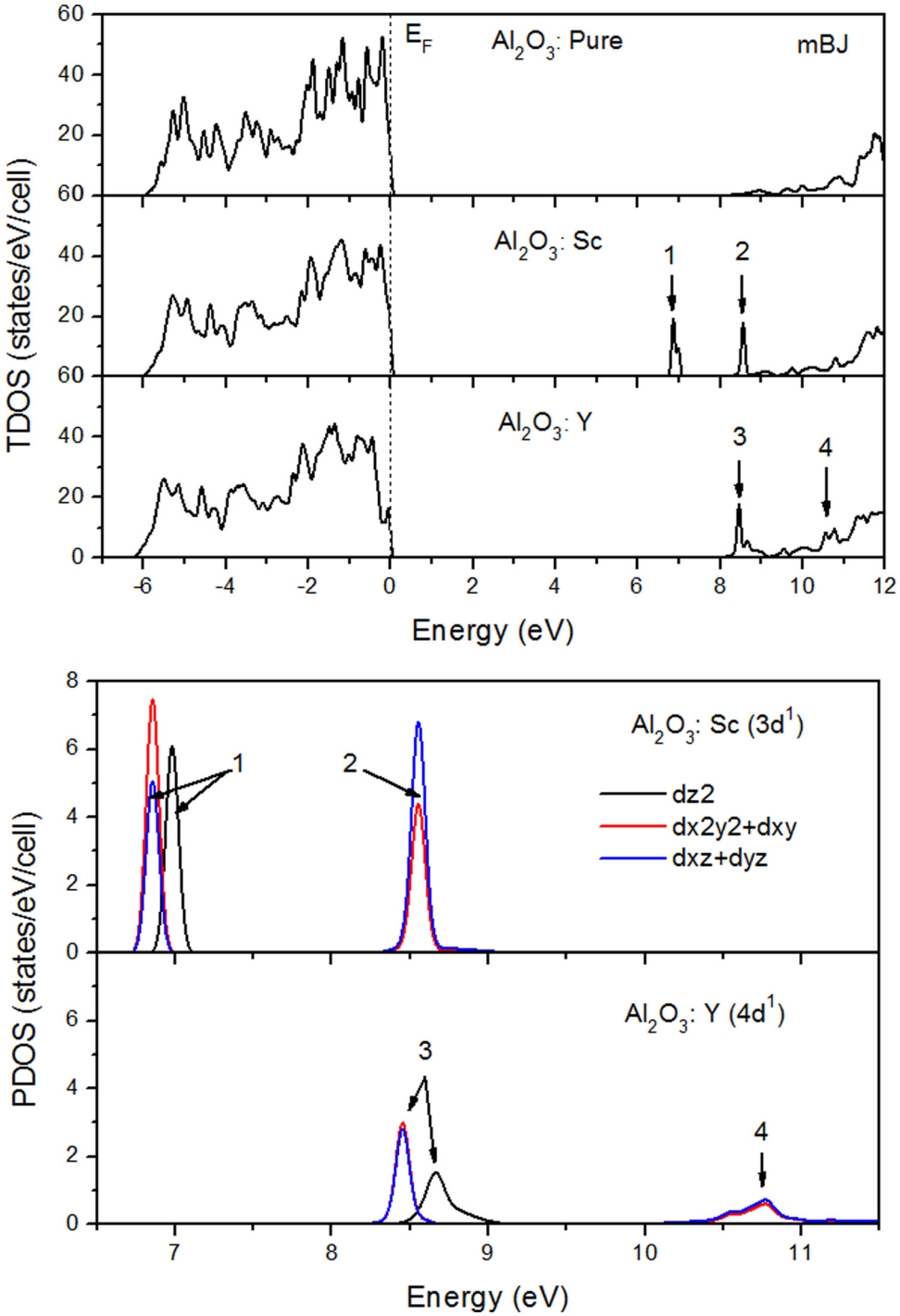

FIG. 2. The theoretical TDOS and PDOS of the Al_2O_3:Sc and the Al_2O_3:Y compounds, calculated by the usage of the mBJ exchange-correlation potential. Numbers 1–4 denote peaks introduced by the 3d-states of the impurities. The lower two graphs show orbital decomposition of these states.

same splitting is much smaller (the splitting between the two peaks dissolved into the peak number 4 and the splitting between the peaks 9 and 10). Besides the octahedral and trigonal crystal field splitting, there exists exchange splitting as well, which is especially pronounced for the energy level E for both the Zr and the Nb impurities (splitting between the peaks 1 and 4 in the first, and between the peaks 6 and 10 in the second case).

C. Optical properties

The information about optical response of all studied systems is accessed from the knowledge of their complex dielectric tensors ε. Imaginary part of this tensor is directly proportional to optical absorption spectrum of the materials. It is possible to compute it knowing the Kohn-Sham eigenvectors and eigenvalues, which are already calculated to produce the electronic band structure (Sec. III B). In the limit of linear optics, neglecting electron polarization effects and within the frame of random phase approximation, the expression for the imaginary part of ε is the following:[23]

$$\varepsilon_{2(\alpha\beta)}(\omega) = \frac{4\pi^2 e^2}{m^2\omega^2}\sum_{i,f}\int_{BZ}\frac{2dk}{(2\pi)^3}|\langle\varphi_{fk}|P_\beta|\varphi_{ik}\rangle||\langle\varphi_{fk}|P_\alpha|\varphi_{ik}\rangle| \times \delta[E_f(k) - E_i(k) - \hbar\omega]. \quad (1)$$

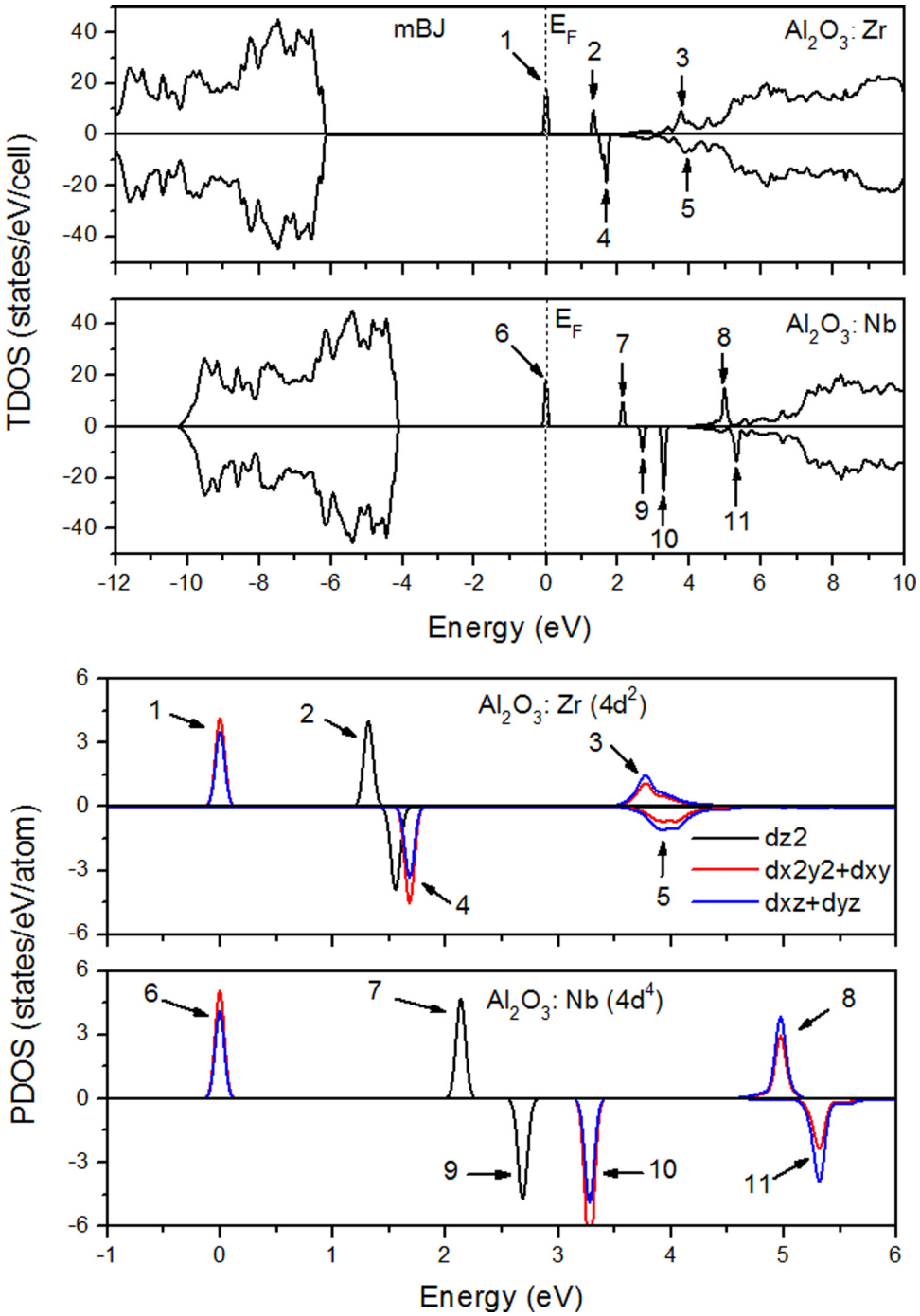

FIG. 3. The theoretical TDOS and PDOS of the Al_2O_3:Zr and the Al_2O_3:Nb compounds, calculated by the usage of the mBJ exchange-correlation potential. Numbers 1–11 denote peaks introduced by the 4d-states of the impurities. The lower two graphs show orbital decomposition of these states.

The formula (1) describes electric dipole allowed transition from the populated Kohn-Sham states $|\phi_{ik}\rangle$ with energy $E_i(k)$ to the empty Kohn-Sham states $|\phi_{fk}\rangle$ of energy $E_f(k)$ with the same wave vector k. The ω is the frequency of the incident radiation, m the electron mass, P the momentum operator, and α and β stand for the incident light polarization directions x, y, z.

Applying the WIEN2k optical package,[24] we computed ε_2 up to incident radiation energy of $\hbar\omega = 40\,\text{eV}$ using the Kohn-Sham states and energies as calculated by both the PBE and the mBJ approaches. The real part of dielectric tensor ε_1 is then determined using Kramers-Kronig relations. Both real and imaginary parts of ε were calculated with a mesh of 38 k-points in the irreducible wedge of the first Brillouin zone, for all five studied systems. Owing to the hexagonal symmetry, the dielectric tensor is diagonal, with two different values: ε_{zz} (along the c-axis of the crystal) and $\varepsilon_{xx} = \varepsilon_{yy}$ (along any direction in the plane perpendicular to the hexagonal c-axis).

Figure 4 serves as a test of reliability of the PBE and the mBJ approaches by comparing the ε_1 and the ε_2 calculated by them with experimental data.[25] It is perceivable that the mBJ calculations correctly reproduce the range and the overall form of the ε_2 spectrum, but underestimate intensity of the low energy absorption peak of the alumina. For that reason, the low energy part of the ε_1 spectrum (especially from

TABLE III. The band gap values of the pure and doped alumina compounds as determined by the PBE and the mBJ calculations (this work) compared with previously published LDA calculations and experimental measurements (available only for the pure system). The calculated PBE and the mBJ magnetic moments of the Zr and Nb impurities are also listed.

	E_g (eV)				μ_{MT} (μ_B)	
	LDA[a]	PBE[b]	mBJ[b]	Expt.[c]	PBE[b]	mBJ[b]
Al_2O_3: Pure	6.10	6.50	8.50	8.80		
Al_2O_3: Sc	5.77	5.80	6.80			
Al_2O_3: Y	6.07	6.40	8.40			
Al_2O_3: Zr	5.58	5.50	6.20		0.388	0.448
Al_2O_3: Nb		4.70	6.30		0.949	1.072

[a]Reference 10.
[b]This work.
[c]Reference 22.

0 to 12 eV) is incorrectly described. On the other hand, the PBE calculations erroneously describe the energy range of the ε_2 spectrum, mostly due to underestimation of the alumina band gap (Table III), but better agree with the low energy part of the experimental ε_1 spectrum.

It might seem that the PBE ε_2 spectrum, with appropriate shift on the energy scale, would provide better agreement with the experiment. This energy shift is usually provided by application of the scissor operator which artificially dislocates the conduction band bottom providing the perfect agreement with the experimental band gap. The problem arises if one studies the imperfect system, with the levels (or bands) that appear within the band gap of the perfect system. In that case, the shift of the conduction band bottom would cause the incorrect description of the positions of the defect states within the gap. Mostly for that reason, we have chosen the mBJ calculations as more appropriate to analyze optical characteristics of the doped alumina systems.

The presence of the Sc, Y, Zr, or Nb impurities in the α-Al_2O_3 crystal matrix mostly affects the absorption edge of the ε_2 spectrum of the doped systems. Figure 5 demonstrates how this edge is changed by the presence of each of the four studied impurities.

Figure 5 clearly shows that the presence of the Y impurity does not change absorption edge of the pure alumina. The presence of the Sc impurity shifts this edge to the lower frequencies, but without changing its form. On the other hand, the Zr and Nb impurities introduce various absorption peaks in the low energy region of the spectrum, changing significantly the absorption edge of the pure alumina. These peaks originate from the electron transitions between the populated *d*-states within the gap and the empty *p*-states of the nearest oxygens at the conduction band bottom, as well as from the populated O *p*-states at the top of the valence band to the empty *d*-states of the impurities within the band gap.

The calculated ε_1 spectra of the defective Al_2O_3:M systems are not presented here because they differ very little from the ε_1 spectra of the pure alumina shown in Figure 4. The reason is a very small impurity concentration considered in our computer simulation. We, however, perceived a small difference in the low energy part of the ε_1 spectra which affects the values of the static dielectric constant (calculated as the ε_1 at the zero energy). Table IV demonstrates the change of the $\varepsilon_1(0)$ in the Y and the Sc doped alumina compared to the $\varepsilon_1(0)$ in the pure alumina compound.

The results in Table IV show that the static dielectric constant exhibits a slight increase when the alumina is doped either with the Y or with the Sc.

IV. CONCLUSIONS

We performed a theoretical study of the Y, Sc, Zr, and Nb doped α-Al_2O_3 with corundum structure. The structural, electronic, and optical properties of the pure and the doped systems have been calculated on the basis of the first-principles, density functional theory based full potential augmented plane wave method. Exchange and correlation effects between electrons have been accounted for in two different ways: (1) by generalized gradient approximation within the PBE parameterization, and (2) by recently developed mBJ approach. Throughout the paper, the PBE and the mBJ results have been confronted, evaluated and compared to the (available) experimental data.

Our principal objective was to verify if the doped materials satisfy two basic conditions for specific application in semiconductor industry:

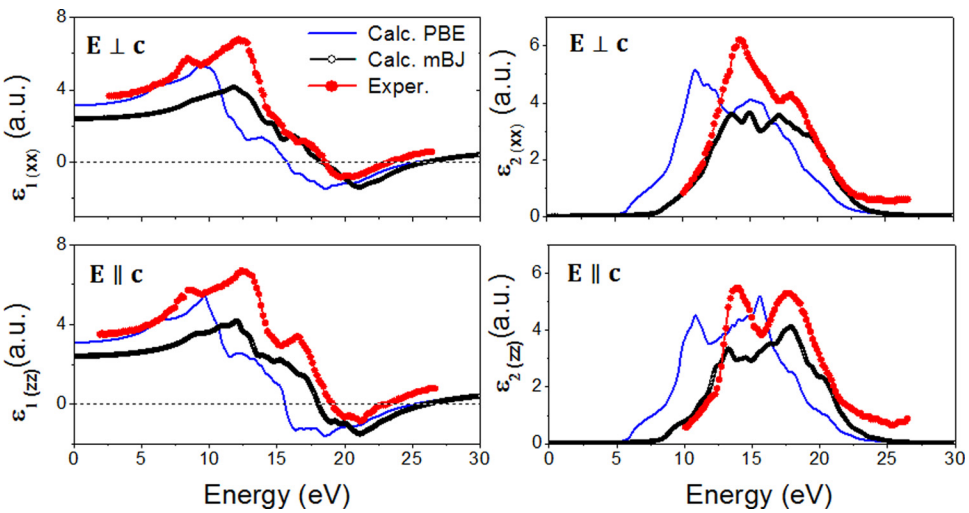

FIG. 4. Real (ε_1) and imaginary (ε_2) part of dielectric tensor of the pure Al_2O_3 calculated using the PBE and the mBJ exchange correlation potential and compared to experimental spectrum.[25] Two situations are considered: when the incident light is polarized (1) along the c-axis and (2) along the axis perpendicular to it.

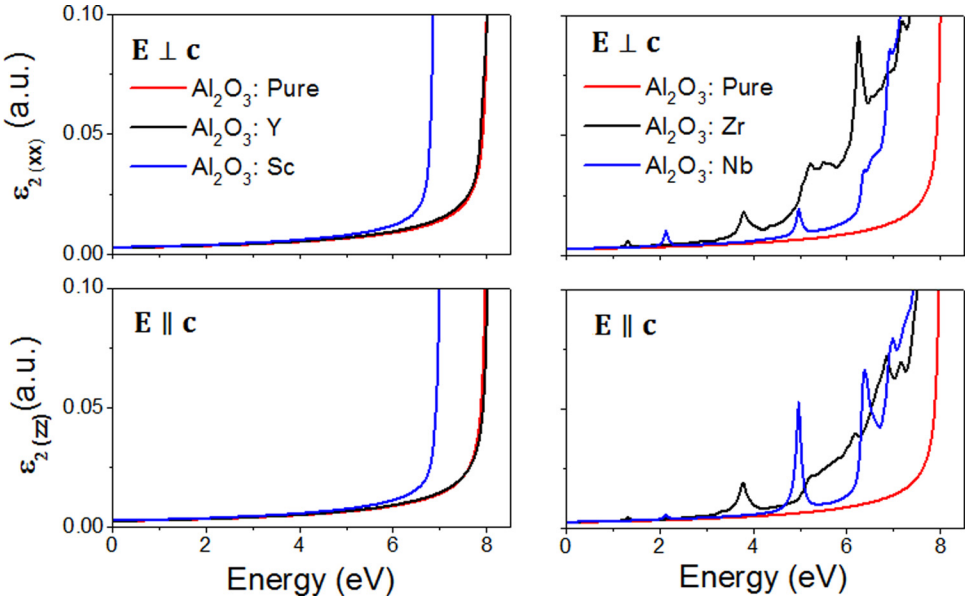

FIG. 5. Modification of the optical absorption edge of the pure Al_2O_3 in the presence of Sc, Y, Zr, or Nb impurities. The ε_2 spectra are calculated by the mBJ approach for the case of the incident light polarized either along the crystalline c-axis (ε_{2zz}) or the axis perpendicular to it (ε_{2xx}).

TABLE IV. Comparison of the static dielectric constant $\varepsilon_1(0)$ of the pure and the Y and Sc doped alumina. For the pure Al_2O_3, the calculated $\varepsilon_1(0)$ is compared to the experimental data and to other theoretical predictions.

	Al_2O_3		Al_2O_3:Y		Al_2O_3:Sc	
	$\vec{E}\perp\vec{c}$	$\vec{E}\parallel\vec{c}$	$\vec{E}\perp\vec{c}$	$\vec{E}\parallel\vec{c}$	$\vec{E}\perp\vec{c}$	$\vec{E}\parallel\vec{c}$
LDA[a]	3.27	2.98				
PBE[b]	3.12	3.08	3.17	3.15	3.25	3.21
mBJ[b]	2.48	2.46	2.50	2.48	2.51	2.49
Expt.[c]	3.06	3.04				

[a]Reference 26.
[b]This work.
[c]Reference 25.

(1) the doping should preserve the size of the gap of the perfect system, as well as the offset of the bands in the near vicinity of it, and
(2) the doping should elevate the static dielectric constant.

From analysis of the electronic structures (Table III, Figs. 1–3) and the optical characteristics (Table IV, Fig. 5) of the pure and the doped alumina systems, we concluded the following.

The Y-doped alumina preserves the size of the band gap of the pure alumina (Table III) and the offset of the bands around it (Fig. 2). The latter is confirmed by the fact that the optical absorption edge of the Al_2O_3:Y does not differ at all from the optical absorption edge of the pure alumina (Fig. 5). At the same time, the static dielectric constant of the doped system elevates its value. Both the PBE and the mBJ approaches lead to the same conclusions.

In the case of the Sc-doped alumina, the mBJ calculations indicate significant decrease of the gap size (Table III, Fig. 2) and significant shift of the optical absorption edge of the pure alumina (Fig. 5). The PBE calculations, on the other hand, result in the much smaller change of the gap size (Table III), but produce very different band offset at the very bottom of the conduction band (Fig. 1): in place of the wide and shallow band of the O 2p-states in the pure alumina it appears a very sharp peak of the Sc *d*-states. Thus, both the PBE and the mBJ calculations indicate "deficiencies" in the electronic structure of the Al_2O_3:Sc, from the point of view of applicability in the semiconductor industry. Due to this fact, a perceived elevation of the static dielectric constant of the Al_2O_3:Sc (Table IV) loses its importance.

In the case of the Zr or Nb doped alumina, there is no any doubt: both the PBE (Table III, Fig. 1) and the mBJ calculations (Table III, Fig. 3) agree that the presence of these impurities significantly diminishes the band gap of the pure system and drastically changes the band offset around it.

Our final conclusion is that only Y-doped α-Al_2O_3 has a potential to be further developed as a high-ε dielectric material, while the Sc-, Zr-, and Nb-doped α-Al_2O_3 do not have that potential. This conclusion is different from the one taken for the κ-Al_2O_3 and amorphous Al_2O_3, in which cases both the Sc- and the Y-doped systems passed the test of applicability as a high-ε dielectric materials.[8,9]

ACKNOWLEDGMENTS

The authors gratefully acknowledge the CNPq and FAPITEC-SE (Brazilian funding agencies) for financial support.

[1]H. H. Tippins, Phys. Rev. B **1**, 126 (1970).
[2]S. Ciraci and I. P. Batra, Phys. Rev. B **28**, 982 (1983).
[3]N. Funamori and R. Jeanloz, Science **278**, 1109 (1997).
[4]J.-F. Lin, O. Degtyareva, C. T. Prewitt, P. Dera, N. Sata, E. Gregoryanz, H.-K. Mao, and R. J. Hemley, Nature Mater. **3**, 389 (2004).
[5]A. I. Kingon, J. P. Maria, and S. K. Streiffer, Nature **406**, 1032 (2000).
[6]G. D. Wilk, R. M. Wallace, and J. M. Anthony, J. Appl. Phys. **89**, 5243 (2001).
[7]P. W. Peacock and J. Robertson, J. Appl. Phys. **92**, 4712 (2002).
[8]M. Haverty, A. Kawamoto, K. Cho, and R. Dutton, Appl. Phys. Lett. **80**, 2669 (2002).
[9]R. Jung, J.-C. Lee, Y.-W. So, T.-W. Noh, S.-J. Oh, J.-C. Lee, and H.-J. Shi, Appl. Phys. Lett. **83**, 5226 (2003).
[10]C. B. Samantaray, H. Sim, and H. Hwang, Appl. Surf. Sci. **239**, 101 (2004).
[11]H. A. R. Aliabad, M. R. Benam, and H. Arabshahi, Int. J. Phys. Sci. **4**, 437 (2009).

[12]W.-Y. Ching, Y.-N. Xu, and M. Ruhle, J. Am. Ceram. Soc. **80**, 3199 (1997).
[13]M. Oetzel and G. Heger, J. Appl. Cryst. **32**, 799 (1999).
[14]O. K. Andersen, Phys. Rev. B **12**, 3060 (1975); D. J. Singh, *Plane Waves, Pseudopotentials and the LAPW Method* (Kluwer Academic, Dodrecht, 1994).
[15]P. Hohenberg and W. Kohn, Phys. Rev. **136**, B864 (1964); W. Kohn and L. J. Sham, Phys. Rev. **140**, A1133 (1965).
[16]P. Blaha, K. Schwarz, G. K. H. Madsen, D. Kvasnicka, and J. Luitz, *An Augmented Plane Waves Plus Local Orbital Program for Calculating Crystal Properties* (Karlheinz Schwarz, Techn. Universität Wien, Austria, 2001).
[17]J. P. Perdew, K. Burke, and M. Ernzerhof, Phys. Rev. Lett. **77**, 3865 (1996).
[18]F. Tran and P. Blaha, Phys. Rev. Lett. **102**, 226401 (2009).
[19]D. Koller, F. Tran, and P. Blaha, Phys. Rev. B **83**, 195134 (2011).
[20]A. F. Lima, S. A. S. Farias, and M. V. Lalic, J. Appl. Phys. **110**, 083705 (2011).
[21]D. J. Singh, Phys. Rev. B **82**, 155145 (2010).
[22]T. V. Perevalov, A. V. Shaposhniko, V. A. Gritsenko, H. Wong, J. H. Han, and C. W. Kim, JETP Lett. **85**, 165 (2007).
[23]M. Bass, E. W. V. Stryland, D. R. Willians, and W. L. Woffe, *Handbook of Optics*, 2nd ed. (McGraw-Hill, New York, 1995), Vol. 1.
[24]C. Ambrosch-Draxl and J. O. Sofo, Comput. Phys. Commun. **175**, 1 (2006).
[25]A. K. Harman, S. Ninomiya, and S. Adachi, J. Appl. Phys. **76**, 8032 (1994).
[26]S.-D. Mo and W. Y. Ching, Phys. Rev. B **57**, 15219 (1998).